Article ID: 1006-8775(2015) 04-0374-15

INFLUENCE OF DIFFERENT-SCALE ERRORS INTERACTIONS ON ANALYSIS AND FORECAST OF REGIONAL NWP MODEL

ZHANG Xu-bin (张旭斌)[1, 2, 3], TAN Zhe-min (谈哲敏)[1]
(1. Key Laboratory of Mesoscale Severe Weather/MOE, and School of Atmospheric Sciences, Nanjing University, Nanjing 210093 China; 2. Guangdong Provincial Key Laboratory of Regional Numerical Weather Prediction, CMA, Guangzhou 510080 China; 3. Institute of Tropical and Marine Meteorology, CMA, Guangzhou 510080 China)

Abstract: In the previous study, the influences of introducing larger- and smaller-scale errors on the background error covariances estimated at the given scales were investigated, respectively. This study used the covariances obtained in the previous study in the data assimilation and model forecast system based on three-dimensional variational method and the Weather Research and Forecasting model. In this study, analyses and forecasts from this system with different covariances for a period of one month were compared, and the causes for differing results were presented. The variations of analysis increments with different-scale errors are consistent with those of variances and correlations of background errors that were reported in the previous paper. In particular, the introduction of smaller-scale errors leads to greater amplitudes in analysis increments for medium-scale wind at the heights of both high- and low-level jets. Temperature and humidity analysis increments are greater at the corresponding scales at the middle- and upper-levels. These analysis increments could improve the intensity of the jet-convection system that includes jets at different levels and the coupling between them that is associated with latent heat release. These changes in analyses will contribute to more accurate wind and temperature forecasts in the corresponding areas. When smaller-scale errors are included, humidity analysis increments are significantly enhanced at large scales and lower levels, to moisten southern analyses. Thus, dry bias can be corrected, which will improve humidity forecasts. Moreover, the inclusion of larger- (smaller-) scale errors will be beneficial for the accuracy of forecasts of heavy (light) precipitation at large (small) scales because of the amplification (diminution) of the intensity and area in precipitation forecasts.

Key words: background error covariances; errors at different scales; data assimilation
CLC number: P435 **Document code:** A
doi: 10.16555/j.1006-8775.2015.04.006

1 INTRODUCTION

In the previous study (Zhang and Tan [1], hereafter ZT12), for a numerical model with a given horizontal resolution, three background error covariances were estimated, including the influences of errors differing in scale. In ZT12, three experiments were conducted to examine the background errors at the given resolution and those introducing influences of errors whose scales are larger and smaller than the given ones respectively. A numerical model (resolution of 12 km) was chosen as the control model to estimate the reference of background error covariances for comparisons, through the NMC method. Following this, forecasts from models whose horizontal resolution was lower and higher than that of the control model were used to produce errors at scales larger and smaller than those determined by the control model respectively. These different-scale errors were introduced into the control model using different nesting techniques, to construct two different impact models. The impact models were used to estimate background error covariances, including influences of different-scale errors using the NMC method.

A comparison showed that the covariances influenced by different-scale errors could reflect the impacts of different-scale dynamic and thermo-dynamic processes in the atmosphere. Consequently, the scale characteristics of these covariances differed. Introducing larger- (smaller-) scale errors into the background error covariances estimated at a fixed resolution changed the univariate variances (magnitude and spectra) and correlation scales as well as multivariate correlations of the original covariances. In addition, the influences of larger-scale errors on the background error covariance estimations differed from those of smaller-scale errors.

Received 2015-03-06; **Revised** 2015-08-28; **Accepted** 2015-10-15
Foundation item: National Natural Science Foundation of China through Grants (41461164008, 41130964); National Key Project for Basic Research (973 Project) (2015452803); Science and Technology Planning Project for Guangdong Province (2012A061400012); China Meteorological Administration (GYHY201406009)
Biography: ZHANG Xu-bin, Ph.D., associate researcher, primarily undertaking research on data assimilation, ensemble forecast and meso- and fine-scale numerical simulation.
Corresponding author: TAN Zhe-min, e-mail: zmtan@nju.edu.cn

When larger-scale errors were introduced, the background error variances increased, particularly at large scales and higher levels. The variances decreased at medium scales and higher levels, whereas they slightly improved at lower levels, particularly at medium and small scales, as smaller-scale errors were introduced. Additionally, introducing larger- (smaller-) scale errors caused larger (smaller) horizontal and vertical correlation scales of the background errors. With regard to multivariate correlations, Ekman coupling was enhanced (reduced) when larger- (smaller-) scale errors were included. Geostrophic coupling in the free atmosphere was weakened under both the conditions.

Background error covariances have profound impacts on the analysis of three-dimensional variational (3DVAR) data assimilation. They determine the weight of the background state in analysis, smooth and spread the observed information by filtering and interpolating spatially respectively. Background error covariances also correct various model variables according to balance relations in the atmosphere (Daley[2]). A detailed discussion of the effects of background error covariances on data analysis can be found in Bannister[3]. However, the impacts of background error covariances with different-scale errors introduced on the analysis and forecast have not been addressed. The single-observation experiments reported in ZT12 indicated that the differences in the different-scale errors introduced resulted in differences in amplitudes and ranges of the analysis increments.

In this study, the three background error covariances estimated in ZT12 were used as the weight matrix in a data assimilation system based on 3DVAR. A series of one-month analysis-forecast experiments with different background error covariances was conducted. Comparisons between corresponding analyses and forecasts are presented in this report to illustrate the impacts of different-scale errors on data analysis and model forecast. In our previous experiments (not shown), the differences of model forecasts longer than 12 h were found to be small. Therefore, to minimize the impact of lateral boundary conditions (LBCs), to maximize the impact of initial conditions (ICs) on model forecast, and to conserve computing resources, the forecast lead-time was set to 12 h.

The remainder of this manuscript is organized as follows. In Section 2, we describe the configurations of the data assimilation and numerical forecast system. The results of the experiments on the impacts of different scale errors on the analyses and forecasts are presented in Sections 3 and 4, respectively. Besides, the corresponding causes are analyzed. Section 5 concludes the manuscript and provides suggestions for future work.

2 MODEL AND EXPERIMENTAL DESIGN

We used the Weather Research and Forecasting (WRF) Advanced Research WRF (WRF-ARW; Skamarock [4]) as the numerical model. The WRF-3DVAR system (Barker[5]) was used as the data assimilation system. In this study, two domains (i.e., D01 and D02 in ZT12) with one-way nesting were used. The model configurations were the same as those for D01 and D02 in ZT12.

ICs of both D01 and D02 at the very beginning of the analysis-forecast cycles (0000 UTC 1 July 2007) are interpolated from National Centers for Environmental Prediction final analysis (FNL) data with 1°×1° horizontal resolution. In the subsequent analysis-forecast cycles at a frequency of 6 h, both ICs and LBCs of D01 were generated by interpolating FNL analyses. The corresponding forecasts were used to provide LBCs for D02. Data assimilation was only performed for D02. During these data assimilation cycles, the background fields were obtained from the 6-h forecast issued from the previous analysis, and the observations were obtained from conventional Global Telecommunications System (GTS) data. Analyses from data assimilation valid at 0000 UTC and 1200 UTC each day were used as the initial fields to issue 12-h forecasts. The first observations were assimilated at 0600 UTC 1 July 2007, and the analysis-forecast cycles continued until 0000 UTC 30 July 2007 (59 cases). The analysis of the experimental results, including the analyses and forecasts, were performed for D02.

Our objective in this paper was to investigate the differences in the impacts of different-scale errors on data assimilation and model forecast. For this purpose, three experiments using background error covariances estimated from ExM, ExL, and ExS in ZT12 were designed and referred to as BeM, BeL, and BeS, respectively. Specifically, the background error covariances employed in BeM included the influences of errors only at fixed-resolution scales, while those employed in BeL (BeS) included the influences of errors at both fixed-resolution and larger (smaller) scales. These three experiments differed only in their background error covariances. Other configurations, such as the assimilated observations and LBCs, were the same. Therefore, the differences of experimental results between BeL (BeS) and BeM can be seen as the impacts of introducing larger- (smaller-) scale errors in the background error covariances.

The qualities of both analyses and forecasts for wind, temperature, and specific humidity were measured by comparing them with radiosonde observations from GTS data, while the quality of forecasts for precipitation

was evaluated by verifying them against the 6-h accumulated precipitation observations obtained from GTS data. The analysis increments, spatial distributions, root-mean-square errors (RMSEs), and biases of the analyses and forecasts for the analysis variables, as well as the verification scores for forecast precipitation, were computed by averaging 59 cases from 1 July until 30 July 2007.

3 RESULTS OF ANALYSES

3.1 *Analysis increments*

Radiosonde innovations (observation minus forecast) of the analysis variables (not shown) reveal some biases in both temperature and humidity in the background fields for all the three experiments. For temperature in the background fields, there is cold bias at lower levels and warm bias at higher levels. In the troposphere, there is dry bias for specific humidity. Consequently, the data assimilations produce positive (negative) analysis increments for temperature at lower (higher) levels and positive increments for specific humidity in the troposphere (not shown). Moreover, the differences in innovations for wind and temperature among the three experiments primarily occur in the middle and upper troposphere, whereas those for humidity are marked at lower and middle levels. Compared with BeM, the magnitudes of the innovations are larger in BeL for both wind and temperature, while those for humidity are larger in BeS.

The absolute analysis increments, defined as the absolute values of the analysis increments are used to measure their magnitude. Figure 1 presents the vertical profiles of the absolute analysis increments averaged over D02. Figures 1a and 1b show that the magnitudes of the analysis increments for wind at middle and upper levels are greater in BeL than in BeM, especially at the level of jet. Compared with BeM, the wind analysis increments in BeS have slightly larger magnitudes at the height of low-level jet in particular for V-wind, while there are marked magnitude reductions at higher levels. The amplitudes of analysis increments for temperature in BeL are the greatest, particularly in the boundary layer and near the tropopause, whereas those in BeS are the smallest, particularly at higher levels (Fig.1c). By contrast with BeM, larger amplitudes of analysis increments for specific humidity are found in BeL, with the most notable improvements in the middle troposphere and boundary layer (Fig.1d). Comparing the increments between BeM and BeS, similar specific humidity magnitudes can be observed, with the exception of smaller increments in the boundary layer in BeS.

These results indicate that background error covariances including influences of larger- (smaller-) scale errors will generate larger (smaller) analysis increments with more pronounced improvements (reductions) at the height where their variances improve (reduce) more noticeably (see ZT12). It is known that analysis increments are determined by background error variances and innovations. In analysis-forecast cycles, wind and temperature innovations are greater when larger-scale errors are introduced into the background error covariances. In addition, background error variances are larger in the corresponding situation. Combining these two factors leads to larger analysis increments. Whereas smaller-scale errors are introduced, there is less obvious variation in the innovations, except for reductions of those for higher-level wind (not shown). In this condition, the background error variances for wind are smaller (larger) at higher (lower) levels (see ZT12). As a consequence, analysis increments for wind are smaller (larger) there. Similarly, smaller background error variances for temperature give rise to smaller increments. For specific humidity, although the corresponding background error variances are moderate, the smaller correlation scale limits the propagation ranges of the innovations.

For further comparison of relative contributions to the analysis increments between different horizontal scales, the power spectra for the analysis increments were calculated (Fig.2). Kinetic energy (KE), internal energy (IE), and latent heat energy (LHE) for analysis increments can be expressed as follows:

$$KE = \frac{1}{2}\left[\overline{(\Delta u)^2} + \overline{(\Delta v)^2}\right] , \tag{1}$$

$$IE = \frac{C_p\overline{(\Delta T)^2}}{T_r} , \tag{2}$$

and

$$LHE = \frac{L^2\overline{(\Delta q)^2}}{C_p T_r} , \tag{3}$$

where Δu, Δv, ΔT, and Δq denote the analysis increments for U-wind, V-wind, temperature, and specific humidity, respectively; C_p=1006.0 J kg^{-1}K^{-1} is the specific heat capacity at constant pressure; T_r=287K is the reference temperature; and L=2.5×10^6 J kg^{-1} is the latent heat of vaporization. The average extends to the entire one-month experimental period.

At higher levels, the relative contributions of the large scales (>1 000 km) are much greater in BeL than in BeM. For both IE and LHE, the relative contributions of the medium-to-small scales (100–500 km) in BeS are slightly lower than those in BeM. This behavior is reversed for the medium-to-large scales (500–1 000 km). Note that the amplitude of KE at medium-to-large scales at the high-level-jet height (around 250 hPa) (Fig.

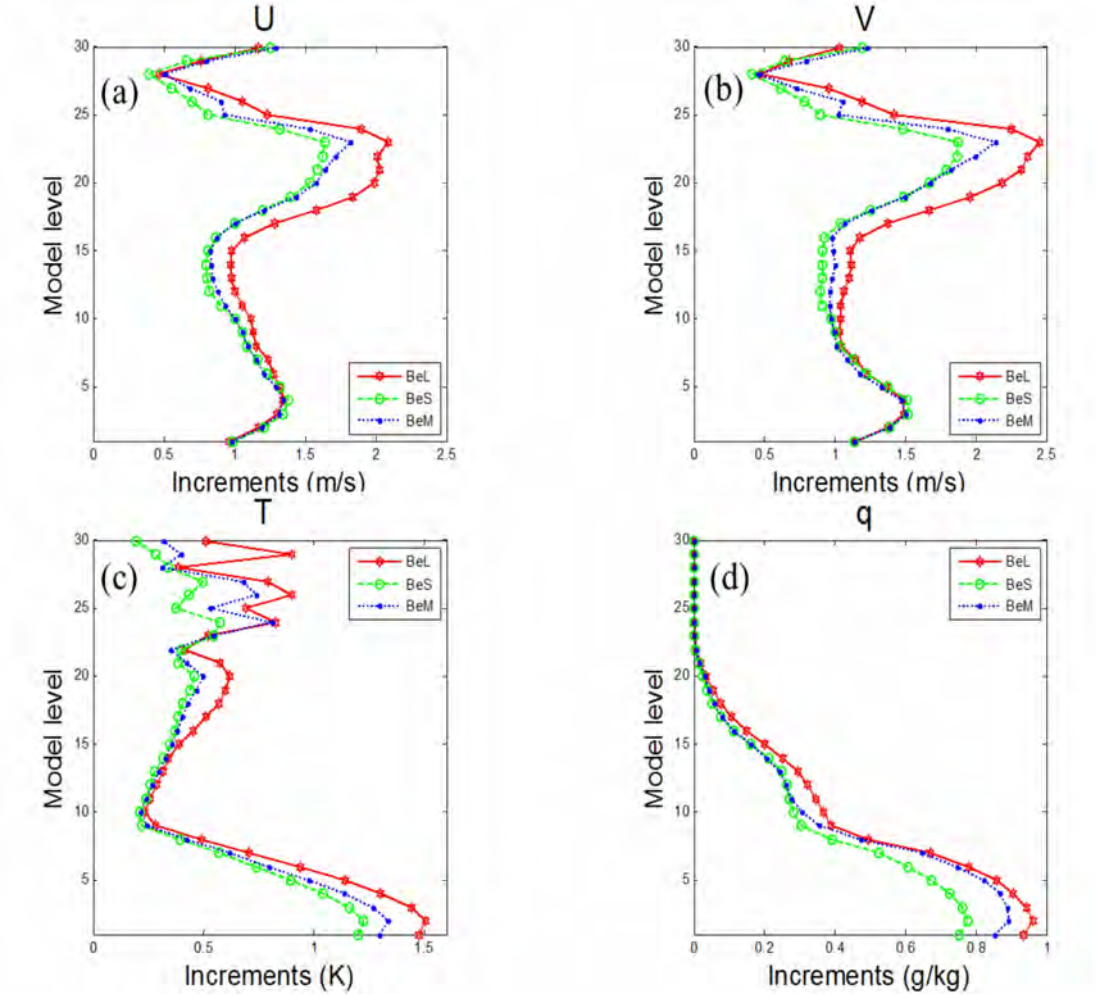

Figure 1. Vertical profiles of the absolute analysis increments in BeL (solid line, hexagrams), BeS (dashed line, circles) and BeM (dotted line, points) for (a) U-wind, (b) V-wind, (c) temperature and (d) specific humidity in D02 domain.

2a) as well as that of LHE at medium scales (100–1 000 km) at middle and higher levels (Fig.2e) is larger in BeS than in BeM.

At lower levels, there are enhanced contributions from the medium and large scales (>300 km) for KE and IE and from the large scales for LHE in BeL, relative to those in BeM (Fig.2b, 2d, and 2f). The contributions from the medium scales are greater in BeS than in BeM. In particular, at the low-level-jet height (approximately 850 hPa), the amplitude of KE at the medium-to-small scales improves evidently (Fig.2b).

In general, the background error covariances influenced by larger- (smaller-) scale errors increase (decrease) the relative contributions of the large (medium) scales to the analysis increments at higher levels and increase those of the large (medium) scales at lower levels. Obviously, the variations in the characteristics of the analysis increments with errors introduced into the background error covariances share some similarities with those of the corresponding variances (see ZT12). However, the differences in innovations among the three experiments contribute to the trivial differences in analysis increments. It is noteworthy that, covariances including the influences of smaller-scale errors produce larger wind analysis increments at medium-to-large (medium-to-small) scales at the height of high-level (low-level) jet accompanied by larger analysis increments for both temperature and humidity at these scales at middle and upper levels. When larger-scale errors are included, the covariances cause humidity analysis increments at large scales and lower levels to increase visibly.

Covariances can impose multivariate balance on analyses. With regard to Ekman pumping (i.e., negative cross-correlations between vorticity and divergence) in the boundary layer, there are stronger negative correlations of analysis increments in BeL than in BeM. These correlations are weaker in BeS as compared to those in BeM, particularly close to the top of the boundary layer (Fig.3). In other words, covariances with larger- (small-

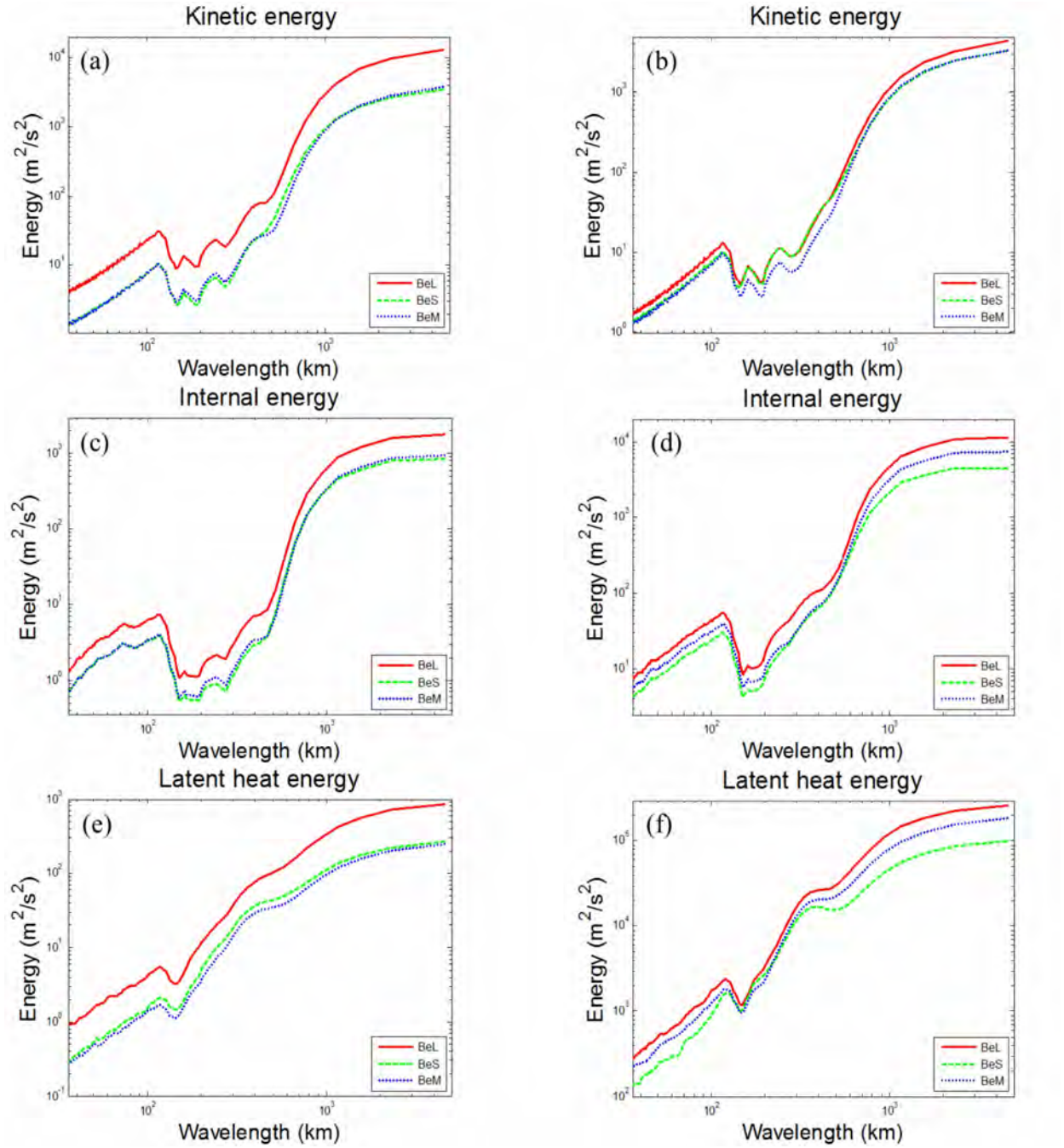

Figure 2. Power spectra in BeL (solid line), BeS (dashed line) and BeM (dotted line) for (a) kinetic energy at level 18, (b) kinetic energy at level 7, (c) internal energy at level 16, (d) internal energy at level 7, (e) latent heat energy at level 16, (f) latent heat energy at level 7.

er-) scale errors introduced tend to strengthen (weaken) the Ekman pumping in analyses. Another perspective of multivariate balance in analyses is geotropic coupling which is enhanced (reduced) at lower (higher) levels after introducing larger-scale errors into covariances, whereas including smaller-scale errors weakens this coupling in the whole troposphere (not shown). To all appearances, the variations in multivariate correlations of analysis increments with errors introduced into the background error covariances share some similarities with those of the corresponding multivariate correlations of the background errors (see ZT12).

3.2 *Analysis errors*

The vertical profiles of RMSEs for the analysis variables averaged over D02 are provided in Fig.4. As shown, analysis errors are smaller in BeL than in BeM. This decrease is due to the larger background error variances in BeL, which cause the analyses to get closer to the observations. There is a reduction in the wind analysis errors in BeS relative to those in BeM, especially at

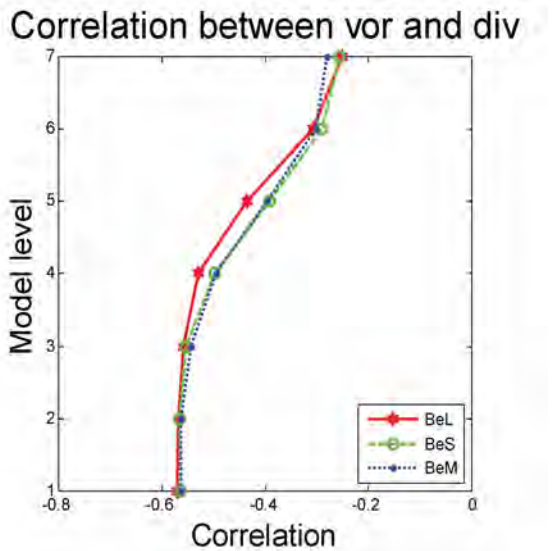

Figure 3. Domain-averaged vertical correlation between the analysis increments of relative vorticity and divergence in BeL (solid line, hexagrams), BeS (dashed line, circles) and BeM (dotted line, points)

the jet levels (Fig.4a and 4b). In BeS, the smaller innovations for wind at higher levels indicate that there are fewer differences between the background fields and observations. Therefore, analyses in BeS tend to approach the observations. Otherwise, larger analysis increments for wind at lower levels attribute to smaller analysis errors there. For temperature RMSEs, the difference between BeS and BeM mainly occurs in the lower troposphere, and the smaller magnitudes occur in the former (Fig.4c) due to the smaller innovations. On comparing the specific humidity RMSEs at lower levels in BeS with those in BeM, we find that they are larger in the former (Fig.4d) because of the smaller analysis increments. As noted above, including larger-scale errors in covariances decreases the analysis errors for all of the analysis variables, whereas including smaller-scale errors decreases the analysis errors for temperature at lower levels and for wind in the whole tropo-

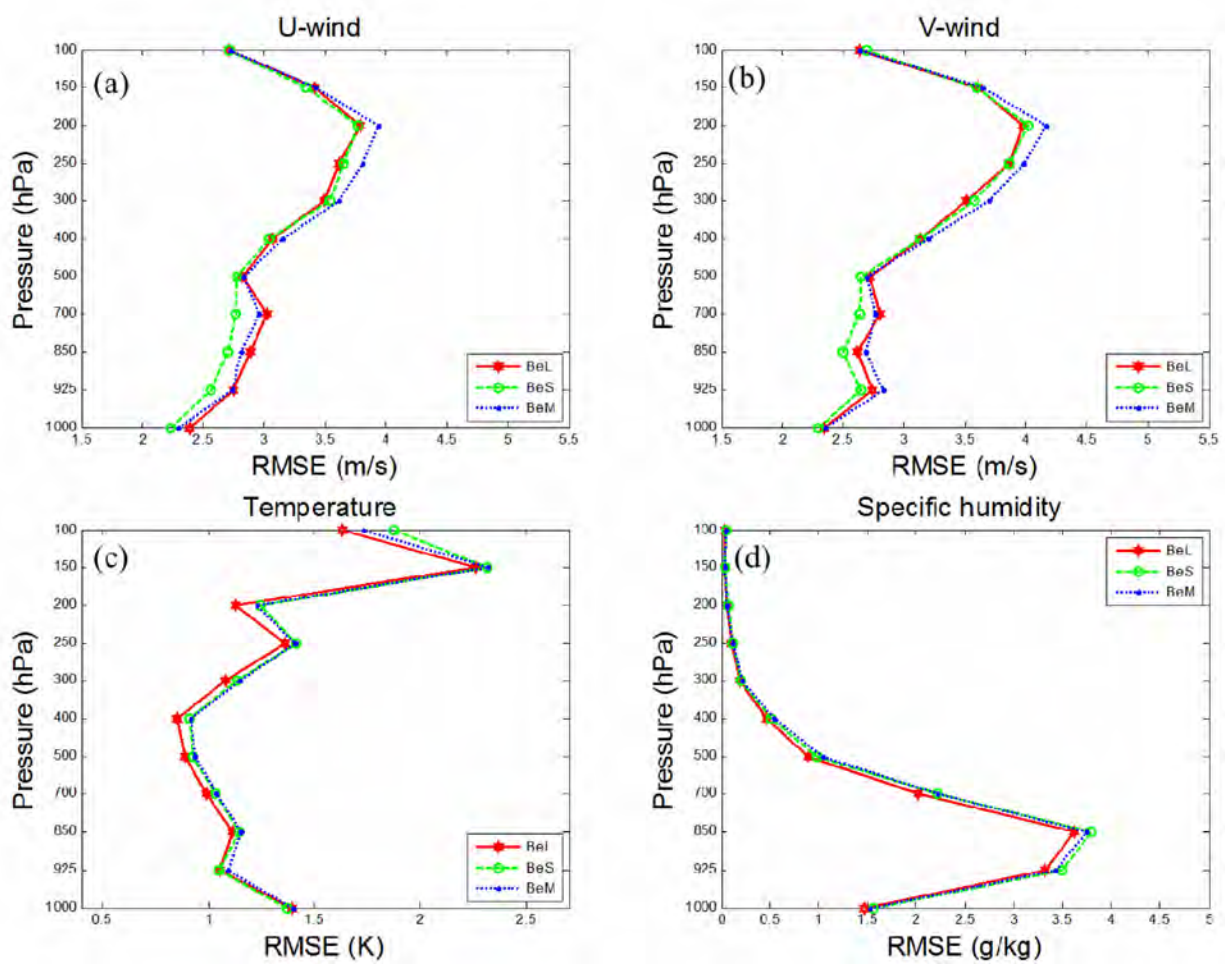

Figure 4. Vertical profiles of RMSE for the analyses with respect to radiosonde observations in BeL (solid line, hexagrams), BeS (dashed line, circles) and BeM (dotted line, points), for (a) U-wind, (b) V-wind, (c) temperature, (d) specific humidity.

sphere but increases the humidity analysis errors at lower levels.

The temperature bias in the middle-level analyses is nearly the same among all of the experiments; while there is larger warm (cold) bias near the surface in BeL (BeS) (Fig.5a). Therefore, analyses in BeL (BeS) strengthen (weaken) the stratification instability at middle and lower levels. Compared with the observations, the analyses have the smallest (largest) amplitudes of dry bias in BeL (BeS). Consequently, the analyses produced with covariances including larger- (smaller-) scale errors are warmer (colder) and wetter (drier) in the middle and lower troposphere in response to the larger (smaller) analysis increments.

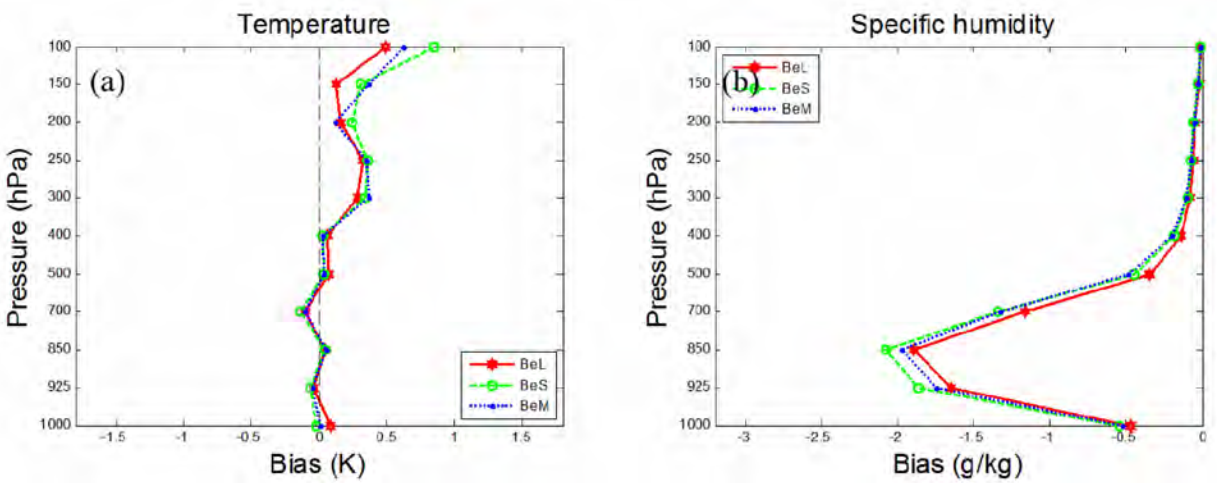

Figure 5. Vertical profiles of bias for the analyses with respect to radiosonde observations in BeL (solid line, hexagrams), BeS (dashed line, circles) and BeM (dotted line, points) for (a) temperature, (b) specific humidity.

3.3 *Analysis fields*

To determine the differences in analyses at different geographical positions and vertical levels among the three experiments, zonal-mean analyses and their differences between BeL (BeS) and BeM were computed (Fig.6).

From Fig.6a and 6b, it is evident that there is a zonal wind extremum at 36°–40° N at level 19–23 (around 250–150 hPa, which corresponds to the high-level-jet height) in both BeL and BeS (Fig.7a). As compared to BeM, the westerly flow is larger in both BeL and BeS. Compared with BeL, the enhancement of the westerly flow in BeS can extend further toward the south and to much lower levels (Fig.6b) and is the most prominent near the high-level-jet height (not shown). At 32°–34°N at level 5–10 (around 250–150 hPa), there are stronger westerly zonal wind corresponding to the low-level jet (Fig.7b) in both BeL and BeS than in BeM, with the strongest wind in BeS (Fig.6b). Compared with BeL, this intensification of the westerly flow in BeS is concentrated in the Yangtze-Huaihe River Basin (not shown). For the southerly flow corresponding to the low-level jet (at 30°–34° N), it is the weakest (strongest) in BeL (BeS) (Figs.6c and 6d). That is, the southerly flow is improved in BeS relative to that in BeM. This improvement is largely located in the Yangtze-Huaihe River Basin (not shown). There is northerly flow north of 35°N in the middle of the troposphere (at levels 9–13) (Figs.6c and 6d). The analyses were averaged zonally over the entire D02; therefore, the weather systems in the northwest, such as the northwest wind which is characterized by cold air at middle levels (not shown), are included in the zonal-mean results. If we exclude the impacts of this northerly flow, there is nearly dominating southerly flow that tilts farther towards the north at higher levels at 34°–38°N in the vertical direction. This southerly flow may match the secondary circulation associated with the coupling between low-level and high-level jets (Liao and Tan[6]). It has the strongest intensity north of the Yangtze-Huaihe River Basin (34°–38°N) in BeS (not shown).

To sum up, analyses using covariances that include smaller-scale errors give rise to stronger westerly jet at higher levels (Fig.7a) and southwesterly jet at lower levels (Fig.7b), as well as the coupling between them in the Yangtze-Huaihe River Basin. As mentioned previously, with such covariances, the wind analysis increments are larger at medium scales at both the high- and low-level-jet heights. This characteristic may lead to stronger jets, particularly jet cores.

At 34°–38°N, the temperatures are higher in BeL and BeS than in BeM in the middle and upper troposphere (around 500–200 hPa) (Fig.6e and 6f). Furthermore, this increase in temperature extends to higher lev-

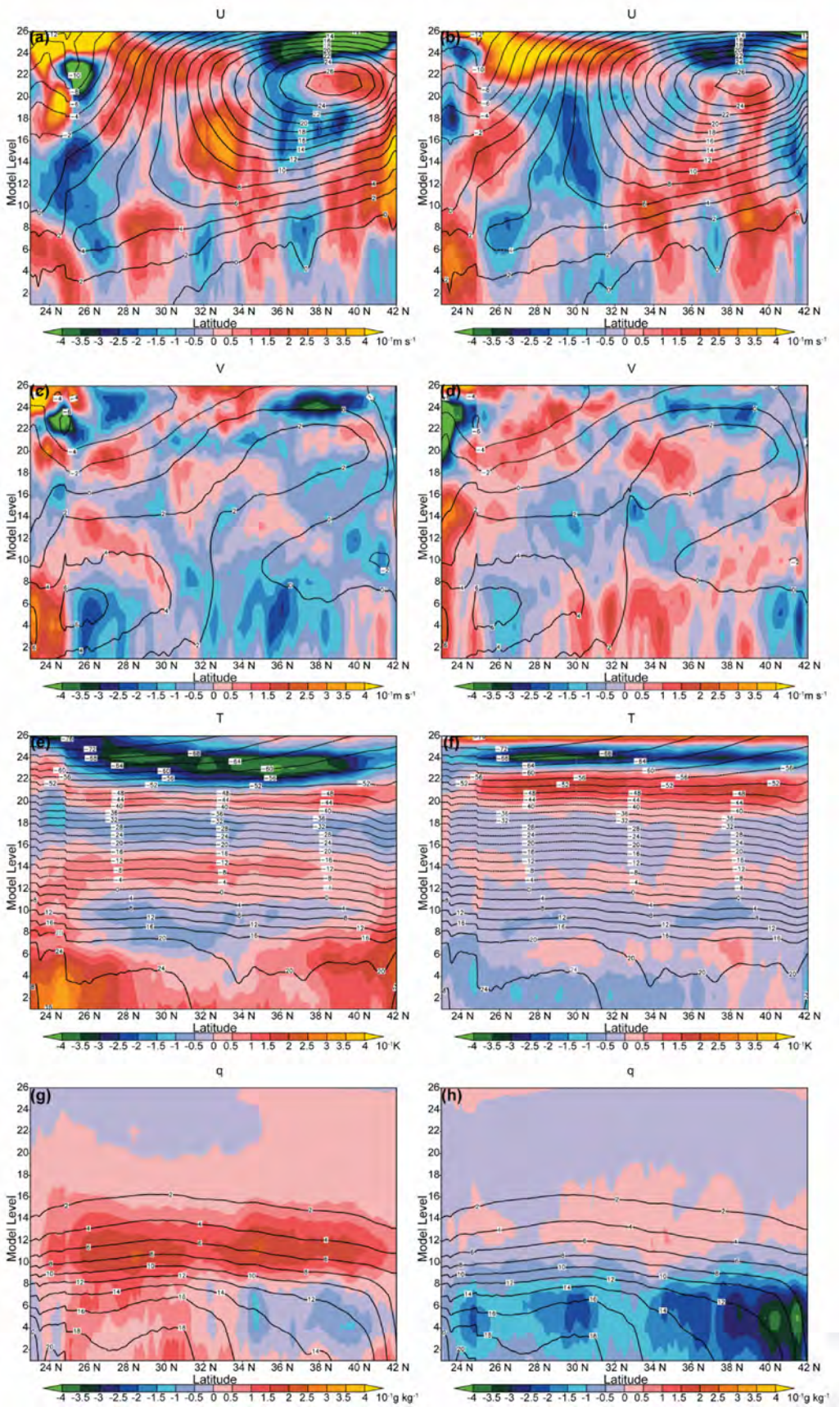

Figure 6. Vertical cross sections of the zonal average analyses (contours, intervals are 2 m/s for U-wind and V-wind, 4 K for temperature and 2 g/kg for specific humidity, positive isolines are solid, negative isolines are dashed) for different experiments and their differences (shaded). Left (right) column shows analyses for BeL (BeS) and differences of analyses between BeL (BeS) and BeM for (a) (b) U-wind, (c) (d) V-wind, (e) (f) temperature and (g) (h) specific humidity.

els in BeS than in BeL and primarily occurs north of the Yangtze-Huaihe River Basin (34°–38°N) (Fig.7c). In the southern portion of D02, the temperature improves in BeL relative to that in BeM at lower levels (below level 7). This enhancement raises stratification instability and horizontal temperature gradient there. In contrast, the temperature decreases in BeS compared with that in BeM. As a result, the horizontal temperature gradient decreases. As shown in Fig.6g and 6h, a humidity enhancement (reduction) occurs at middle and lower levels (below level 12) in the southern portion of D02 in BeL (BeS) compared with that in BeM. The most striking variations are located in the southeast of D02 where the southwesterly flow has a high intensity (Fig.7d). These variations are concentrated at middle (lower) levels in BeL (BeS). In central D02, the humidity gradient increases (decreases) at lower levels in BeL (BeS) compared with that in BeM.

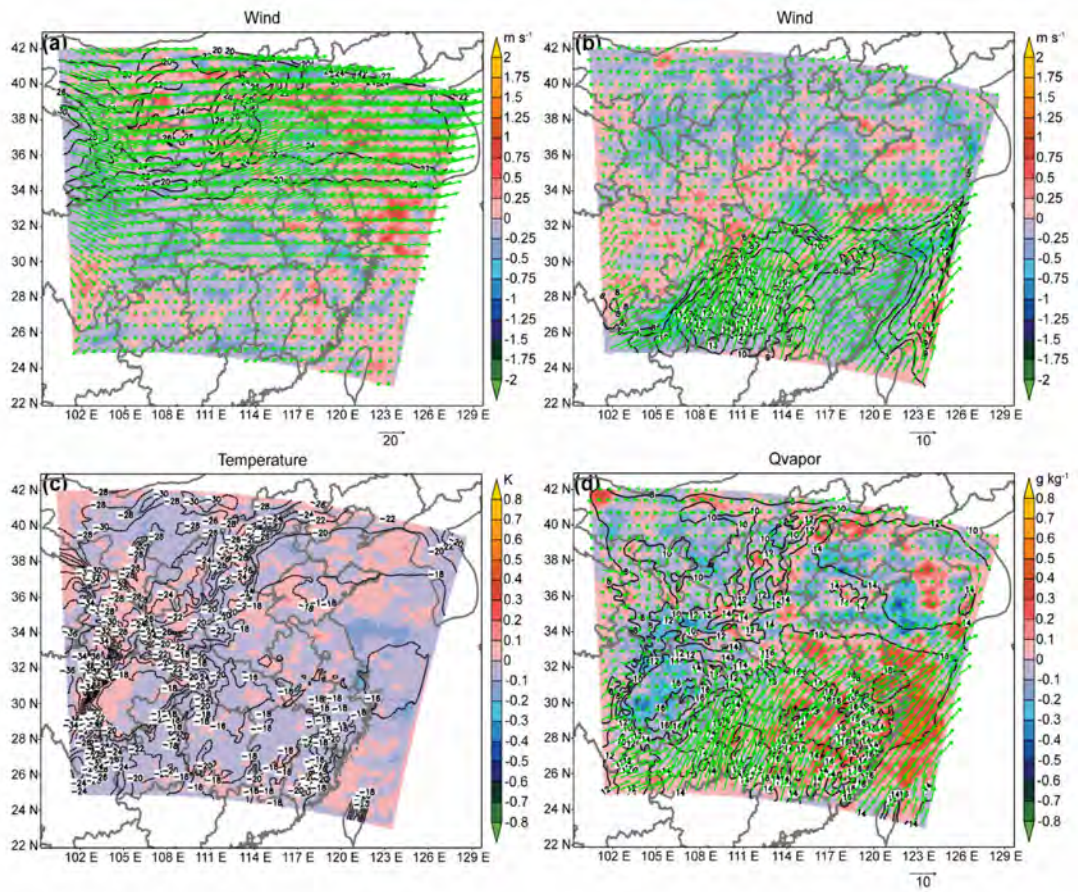

Figure 7. Horizontal distributions of the analyses (contours, intervals are 2 m/s for wind at level 18 and 1 m/s for wind at level 7, 2 K for temperature and 2 g/kg for specific humidity, positive isolines are solid, negative isolines are dashed; vectors are wind) for different experiments and their differences (shaded). (a), (b) and (c) show analyses for BeS and differences of analyses between BeS and BeM while (d) show analyses for BeL and differences of analyses between BeL and BeM for (a) wind velocity at level 18, (b) wind velocity at level 7, (c) temperature at level 16 and (d) specific humidity at level 7.

In summary, the analyses using covariances which include smaller-scale errors lead to higher temperature at middle and upper levels warming may be due to latent heat of condensation released from convection. Under such circumstances, there are larger analysis increments at the medium-to-large scales for both IE and LHE at middle and upper levels. This characteristic may explain the increased latent-heat release, which is accompanied by higher temperature there. On the other hand, this warming corresponds well with the secondary circulation in space. So it seems that, there may be interactions between the latent heat of condensation released from convection and the coupling of high-level jet with low-level jet; in other words, convection is attributed to ascending motion in the secondary circulation and can intensify the coupling between high- and low-level jets (Liao and Tan[6]). The horizontal gradients for both temperature and humidity are smaller in this case. The analyses yield higher temperature and humidity at lower levels in the southern part of D02 when the corresponding covariances are influenced by larger-scale errors. This result is related to the larger amplitudes of both the temperature and humidity analysis increments and to the larger scales of them depicting large-scale

advection very well.

4 RESULTS OF FORECASTS

4.1 *Forecasts for analysis variables*

The forecast errors, measured by RMSEs, were calculated for all the three experiments (Fig.8) to evaluate the differences in forecasts for analysis variables between different experiments. Compared with BeM, BeS improves (i.e., reduces RMSEs) the wind forecasts, with the greatest improvements at the heights of both higher- and lower-level jet, whereas BeL degrades the forecasts (Fig.8a and 8b). In the temperature forecasts, BeS produces the lowest RMSEs, while BeL produces the highest. Figure 8d shows that the humidity forecast errors are somewhat smaller (larger) in BeL (BeS) than in BeM, especially at middle and lower levels. In conclusion, forecasts in BeS better predict wind and temperature, while those in BeL are more skillful for humidity at middle and lower levels.

Throughout the troposphere, forecast biases of temperature are greater (smaller) in BeL (BeS) than in BeM (Fig.9a). The humidity is lower in the forecasts than in the background fields for all of the experiments, and this dry bias reaches the lowest (greatest) degree in BeL (BeS), particularly at middle (lower) levels (Fig.9b).

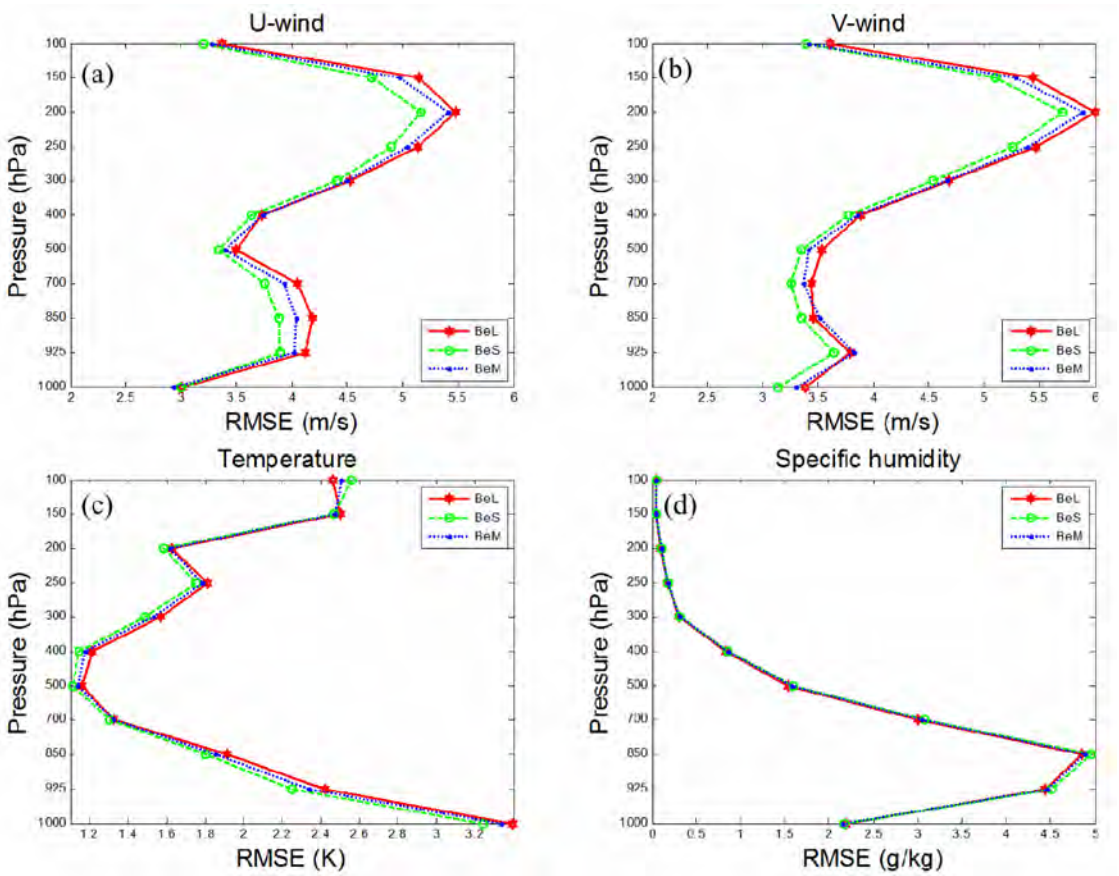

Figure 8. Vertical profiles of RMSE for the 12-h forecasts with respect to radiosonde observations in BeL (solid line, hexagrams), BeS (dashed line, circles) and BeM (dotted line, points) for (a) U-wind, (b) V-wind, (c) temperature, (d) relative humidity.

The previous discussion illustrates that both BeL and BeS can improve the forecast performance for some variables compared with that obtainable by BeM. However, the extent of the improvements may differ depending on the geographic area. To investigate this dependence, we compared the extent of the improvements in different geographic areas for BeL and BeS. Different geographic areas in D02 (hereafter called the sub-area) were selected. Area-mean forecast errors (specifically, the RMSEs) for all of the stations in the sub-area and all of the experiments were calculated. The differences of the RMSEs averaged over sub-areas or over the entire D02 between BeL (BeS) and BeM were used to represent the forecast improvements in the corresponding areas (Table 1). At 200 hPa, the region in which the horizontal wind velocity exceeds 30 m/s (that is, the horizontal wind is a high-level jet) is defined as a sub-area for U-wind at higher levels. At 850 hPa, the region in which the horizontal wind velocity exceeds 12 m/s (that is, the horizontal wind is a low-level jet) is defined as a sub-area for both U-wind and V-wind at lower levels. As can be seen in Table 1, the extent of improvement for wind in BeS is greater

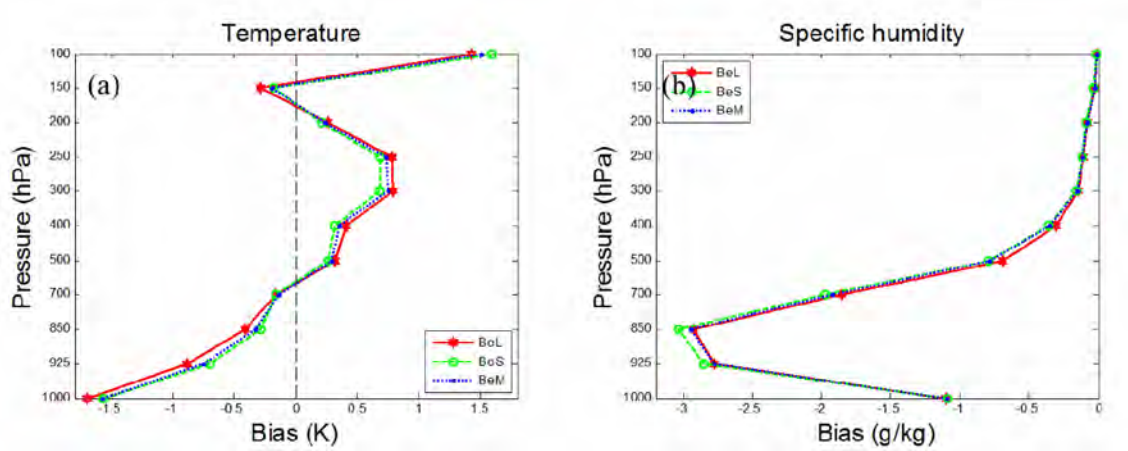

Figure 9. Vertical profiles of bias for the 12-h forecasts with respect to radiosonde observations in BeL (solid line, hexagrams), BeS (dashed line, circles) and BeM (dotted line, points) for (a) temperature, (b) specific humidity.

in areas with high- or low-level jet than that in D02 as a whole. We defined the area to the north of the Yangtze-Huaihe River Basin at 300 hPa in which the secondary circulation is stronger as a sub-area for V-wind at higher levels. Similarly, the extent of improvement in BeS is greater for V-wind in this sub-area compared with that in D02 as a whole. At 400 hPa, the corresponding sub-area is located in the area with higher temperature. In space, this sub-area is similar to that for V-wind at higher levels. From Table 1, it is evident that BeS improves the temperature forecasts to a greater extent in this sub-area than in D02 as a whole. The forecast improvements for wind and temperature in BeS are concentrated in the regions with jet streams and their corresponding secondary circulation. The moister area in the south of D02 at 850 hPa is defined as the sub-area for humidity at lower levels. It is evident that BeL results in more significant forecast improvements for humidity in the south of D02 than in other areas.

From these results, it is evident that BeS analyses generate stronger high- and low-level jets, as well as jet stream coupling. For this reason, analyses for wind in these regions may be depicted more reasonable to improve the corresponding forecasts. Additionally, greater amounts of latent heat are released at middle and upper levels, which correspond well with stronger secondary circulation to be benefit to predicting temperature there. BeL analyses well represent the influence of large-scale advection on moisture that causes increased humidity in the south at middle and lower levels. Thereby, the dry bias for analyses in those regions and levels is alleviated, improving the humidity forecasts.

Table 1. Differences of RMSE averaged over the whole domain or the subarea of D02 between different experiments. Values of differences smaller in subarea than in D02 are shown in boldface. U-wind at 200 hPa is averaged over the areas where wind velocity is larger than 30 m/s; V-wind at 300 hPa is averaged over the areas located at 110°–124°E and to the north of 30°N; U-wind and V-wind at 850 hPa are averaged over the areas where wind velocity is larger than 12 m/s; Temperature at 400 hPa is averaged over the areas to the east of 114°E and to the north of 30°N; specific humidity at 850 hPa is averaged over the areas to the south of 33°N.

	U (200 hPa) (ms^{-1})	V (300 hPa) (ms^{-1})	U (850 hPa) (ms^{-1})	V (850 hPa) (ms^{-1})	T (400 hPa) (K)	q (850 hPa) (gkg^{-1})
L–M (All)	0.0322	0.0308	0.1345	–0.0431	0.0329	–0.0418
L–M (Sub)	–0.0406	0.0750	0.3126	–0.0573	0.0467	–0.0458
S–M (All)	–0.2237	–0.1197	–0.1454	–0.1855	–0.0375	0.0710
S–M (Sub)	–0.3081	–0.1536	–0.1239	–0.3572	–0.0435	0.0152

4.2 *Traditional verification of precipitation*

Traditional statistics (Jolliffe and Stephenson [7]; Wilks [8]) have been widely used to verify Quantitative Precipitation Forecast (QPF). The most commonly used statistics include the Equitable Threat Score (ETS) or Gilbert Skill Score (GSS), Frequency Bias (FB), Probability of Detection (POD), and False Alarm Rate (FAR).

The ETS measures the fraction of events that are correctly predicted compared with those that are either predicted or observed, accounting for hits due to ran-

dom chance. Larger ETS values indicate more accurate QPF. QPF is considered to be perfect when the corresponding ETS equals 1. The FB is the ratio of forecast events to observation events (optimal value is 1). FB values greater (less) than 1 indicate that forecasts overestimate (underestimate). The POD measures the fraction of events correctly predicted to occur (optimal value is 1). The FAR is the proportion of events predicted to occur but not observed (0 indicates the best forecast).

These verification scores were calculated for forecasts of 6-h accumulated precipitation and were averaged over the corresponding results for 6-h and 12-h forecasts (Fig.10). Overall, the ETS decreases as the precipitation threshold increases. Therefore, the model appears to prefer predicting lighter precipitation. BeS outperforms BeM for light precipitation (0–15 mm), and this improvement persists for heavier precipitation (20–25 mm). BeL shows appreciable forecast improvement over BeM only for much heavier precipitation (30 mm) (Fig.10a). It is evident that light precipitation is overestimated in all forecasts. The QPF overestimated (underestimated) heavy precipitation (20–30 mm) in BeL (BeS) (Fig.10b). In other word, the most serious precipitation overestimation (underestimation) occurs in BeL (BeS). Besides, the POD is low and the FAR is high for heavy precipitation in all the forecasts; however, the opposite results (i.e., high POD and low FAR) are evident for light precipitation. Generally, results of POD are nearly equal for all experiments (Fig.10c). Nevertheless, the POD is marginally higher for light (much heavier) precipitation in BeS (BeL) than in BeM. The FAR is lowest in BeS and highest in BeL (Fig.10d).

As shown, the POD values are similar, while the FB shows greater variation among the three experiments. Therefore, it is clear that there are some differences in the area of precipitation. Specifically, BeL (BeS) predicts larger (smaller) precipitation area. In addition, the improved forecasts of much heavier precipitation in BeL are due to the higher POD and lack of underestimate, whereas the higher FAR and overestimation lead to poor forecasts of light precipitation. In BeS, the higher POD, lower FAR, and overestimation of light precipitation contribute to better forecast performance. A decrease in forecast skill for heavy precipitation, which is attributed to remarkable underestimation, is found in BeS.

4.3 *Spatial verifications of precipitation*

Recently developed spatial verification methods (Hoffman et al.[9]; Ebert and McBride [10]; Casati et al.[11];

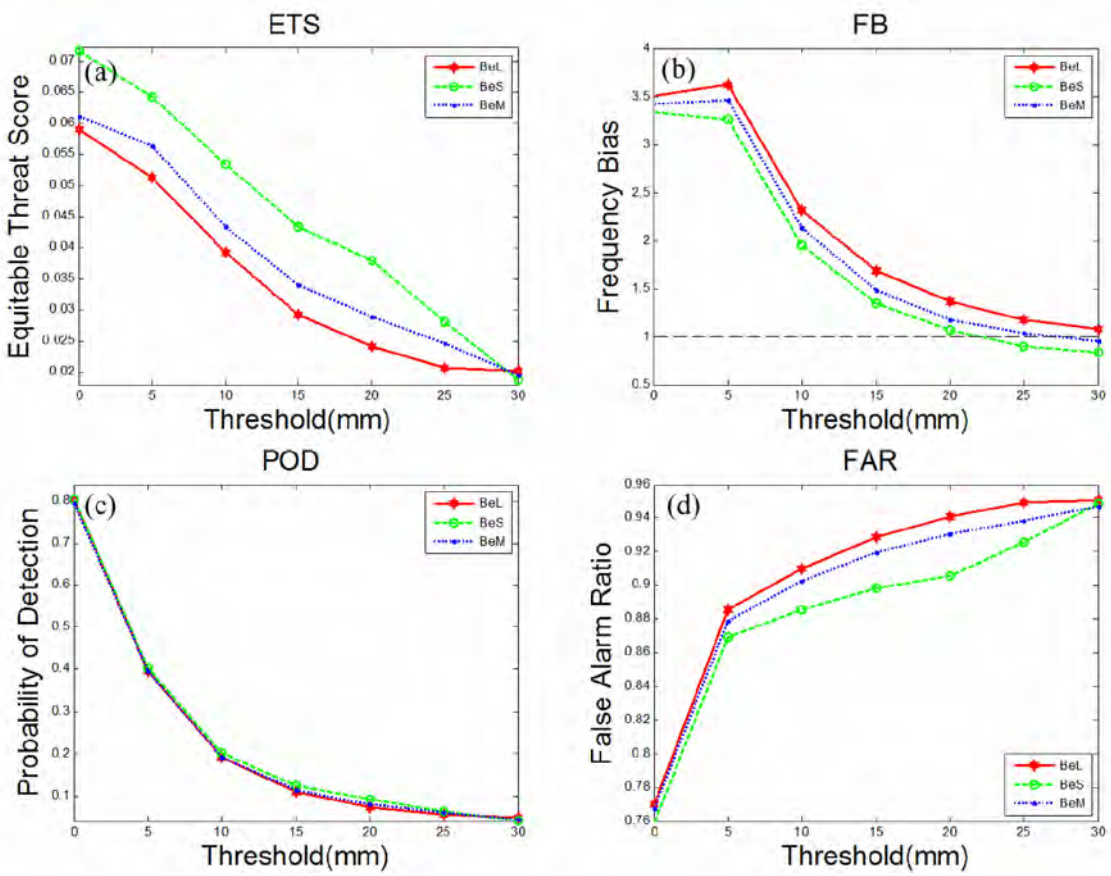

Figure 10. Verification scores for forecasts of the 6-h accumulated precipitation averaged over the 6 h and 12 h forecasts as a function of precipitation threshold (mm) in BeL (solid line, hexagrams), BeS (dashed line, circles) and BeM (dotted line, points). Scores are (a) ETS, (b) FB, (c) POD and (d) FAR.

Davis et al.[12]; Roberts and Lean[13]) do not require forecasts to match observations exactly at fine scales exactly. Accordingly, these new methods can reduce the representativeness error (Tustison et al.[14]) to some extent. Neighborhood-based verification approaches only require approximate agreement between forecasts and observations in space and time in the matching process (Theis et al.[15]; Ebert [16]). These approaches compare all the points of the forecasts with those of the observations in space-time neighborhoods relative to a point in the observation field using the global properties, such as the mean, of the fields within the neighborhoods. Then, the differences between the forecasted and observed values of these properties are used to measure the degree of matching. The Fractions Skill Score (FSS) (Roberts and Lean[13]; Roberts[17]; Mittermaier and Roberts[18]) is based on these approaches and can be used to evaluate the forecast skill at different scales. The FSS is calculated for different precipitation thresholds and neighborhood sizes to reflect the forecasting skill for different precipitation intensities and scales (see Roberts and Lean 2008 for the detail calculation of FSS). Note that FSS values range from 0 to 1. A forecast with perfect skill has a score of 1; a score of 0 indicates no skill. As the FSS value increases, the corresponding forecast skill also increases.

Figure 11 shows the FSS for forecasts of the 6-h accumulated precipitation. For the light precipitation forecasts, those obtained from BeS (BeL) have higher (lower) quality than those obtained from BeM at all scales (Fig.11a and 11b). More importantly, this behavior is more evident at larger scales, which indicates better forecast performance in location and pattern of light precipitation in BeS. For heavier precipitation, the forecast skill of BeS is higher than that of BeM at small scales (0–150 km). However, this improvement is not apparent at large scales (150–250 km). The fact that the greatest differences between BeS and BeM occur at small scales implies a higher forecast skill for the locations of heavier precipitation in BeS. In BeL, forecast performance of heavier precipitation is slightly better (worse) than that in BeM at large (small) scales (Fig. 11c). At all scales, BeL attains the forecast skill for much heavier precipitation that is much higher than that of BeM (Fig.11d). Their differences are more noticeable at larger scales, reflecting the advantage of BeL in predicting the location and pattern of intense precipitation. Overall, the forecast skill for this type of precipitation is

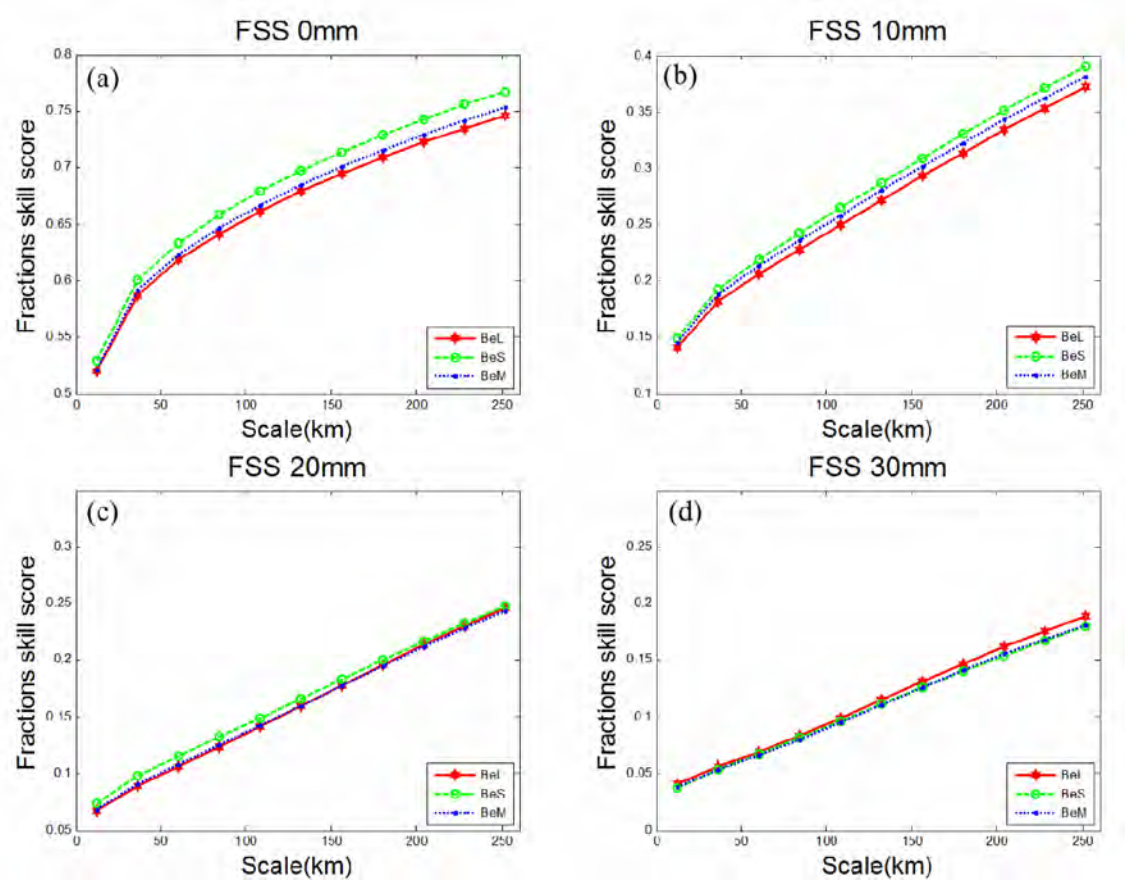

Figure 11. FSS for forecasts of the 6-h accumulated precipitation averaged over the 6 h and 12 h forecasts as a function of horizontal scale for thresholds of (a) 0 mm, (b) 10 mm, (c) 20 mm, and (d) 30 mm in BeL (solid line, hexagrams), BeS (dashed line, circles) and BeM (dotted line, points).

very similar in BeS and BeM (Fig.11d). In general, BeL (BeS) predicts heavy (light) precipitation at large (small) scales better than BeM does.

4.4 *Discussion on precipitation forecast*

The results of both traditional and spatial precipitation verification indicate that forecasts of precipitation show different characteristics when the corresponding background error covariances are influenced by errors at different scales. To be more specific, the model with covariances that include the influences of larger- (smaller-) scale errors predicts larger (smaller) area of precipitation and seriously overestimates (underestimates) light (heavy) precipitation. Additionally, under these conditions, such models show better forecast performances for heavy (light) precipitation at large (small) scales.

It is difficult for a numerical model to predict precipitation accurately, particularly the intense precipitation, because initial fields cannot accurately describe conditions that favor the formation and development of rainfall in the real atmosphere. These conditions include unstable stratification, sufficient moisture and strong ascending motion. As mentioned previously, analyses are wetter (drier) with more (less) unstable stratification, and the analysis increments have stronger (weaker) Ekman pumping in BeL (BeS). In addition, the relative contribution to the analysis increments for LHE is greater at large (medium) scales. As a consequence, the corresponding analyses produce humidity fields that feature larger (smaller) spatial ranges. Finally, the combination of the above factors results in larger (smaller) intensity and area of precipitation in BeL (BeS) forecasts.

If the moisture distribution in the initial field is real, the larger (smaller) precipitation intensity in BeL (BeS) forecast will lead to the smaller (larger) underestimation of heavy precipitation and thus improve (reduce) the corresponding forecast skill. In contrast, the larger (smaller) overestimation and more (fewer) false alarms in BeL (BeS) forecasts contribute to the worse (better) forecast performance of light precipitation. For forecasts of large-scale precipitation, the better (worse) performance in BeL (BeS) is due to its larger (smaller) area of precipitation. The opposite is true for small-scale precipitation. If there is a pseudo-distribution of moisture in the initial field, stronger development of moisture perturbation in BeL will give rise to larger overestimations in precipitation forecasts, which reduces the performances of forecasts for both heavy and light precipitation. However, this degradation in BeS is not so serious because of its weaker development of moisture perturbation.

5 CONCLUSIONS AND DISCUSSIONS

Expanding on the work presented in ZT12, the background error covariances estimated at specified-resolution scales, as well as those including the additional influences of errors with larger (smaller) scales than the specified ones in ZT12, were employed in the WRF 3DVAR data assimilation system. Data assimilation with different background error covariances followed by WRF forecasts was performed to compare the impacts of covariances with different-scale errors on data analysis and model forecast.

The analysis-forecast cycles for a one-month period show that the covariances influenced by different-scale errors correspond to analysis increments with different features. In response to covariances that introduced the influences of larger- (smaller-) scale errors, the analysis increments increase (decrease). Moreover, the introduction of larger-scale errors enhances the contributions of large scales to the analysis increments, whereas the medium-scale analysis increments contribute much more (less) at lower (higher) levels when smaller-scale errors are introduced. In the former case, the analysis increments for moisture generated at lower levels obviously increase the magnitude at large scales. In the latter case, the magnitudes of the analysis increments for wind generated at the heights of high- and low-level jets improve at medium-to-large and medium-to-small scales respectively, in conjunction with the improvement of analysis increments for temperature and moisture at middle and upper levels. Additionally, larger (smaller) ageostrophic components at lower (higher) levels and stronger Ekman pumping are apt to be produced in analysis increments when covariances including larger-scale errors; whereas the ageostrophic component is enhanced at most levels when covariances that include smaller-scale errors. In summary, the characteristics of the analysis increment variations with different-scale errors introduced in the background errors are similar to those reported in ZT12 for covariances under the corresponding conditions.

For all the variables, the analysis errors reduce in the context of covariances with larger-scale errors. Accounting for the influences of smaller-scale errors, analysis errors for wind and lower-level temperature decrease, while it is on the contrary for lower-level humidity. In the east of analyses, especially in the Yangtze-Huaihe River Basin, the high- and low-level jets and jet stream coupling, as well as the latent heat of condensation at middle and upper levels strengthen when the covariances include smaller-scale errors. In the southern analyses, the introduction of larger- (smaller-) scale errors leads to warming (cooling) and wetting (drying), which increases (decreases) the corresponding stratification instability and horizontal temperature and humidity gradients.

Variations were observed in the forecasts due to

the differences in analyses caused by the dissimilar influences of the covariances with errors at different scales. When larger-scale errors are introduced, the humidity forecasts at middle and lower levels show better performance. This improvement is concentrated in the south. When smaller-scale errors are included, the wind and temperature forecast skills are higher. This positive impact was greatest in the eastern areas where high- and low-level jets and jet stream coupling exist.

Furthermore, the covariances with larger- (smaller-) scale errors cause the model to predict larger (smaller) intensity and area of precipitation and to overestimate (underestimate) light (heavy) precipitation more seriously. As a result, the forecast quality improves for heavy (light) precipitation at large (small) scales.

In this study, radiosonde observations assimilated in the analysis process were used to verify the analyses. Thus, the resulting analysis errors measured how well the analyses fit the observations for independent verification at the analysis time (Zhang et al.[19]). To appropriately compare the analysis errors corresponding to different covariances, we will consider using observations rather than GTS data to verify analyses in the future.

The covariances that include different-scale errors have different impacts on the model analyses and forecasts. It is worth noting that, these discrepant impacts complement each other in forecast performance. For example, the model with covariances influenced by larger-scale errors more accurately predicts heavy precipitation, while the model influenced by smaller-scale errors better predicts light precipitation. Hence, in the future, to better predict summer precipitation in eastern China using data assimilation, we will combine background errors including larger-scale errors with those including smaller-scale errors to construct an optimal estimate of covariances that includes the combined influences of these two types of errors.

REFERENCES:

[1] ZHANG Xu-bin. A Study on the mutil-scale background error covariances in 3D-Var data assimilation [D]. Doctoral thesis, Nanjing University, 2012.

[2] DALEY R. Atmospheric data analysis [M]. Cambridge: Cambridge University Press, 1991, 1-457.

[3] BANNISTER, R N. A review of forecast error covariance statistics in atmospheric variational data assimilation. I: Characteristics and measurements of forecast error covariances [J]. Quart J Roy Meteorol Soc, 2008, 134: 1 951-1 970.

[4] SKAMAROCK W C, KLEMP J B, DUDHIA J, et al. A description of the Advanced Research WRF version 2 [R]. NCAR Tech. Note NCAR/TN-468_STR, 2005: 88 pp.

[5] BARKER D M, HUANG W, GUO Y R, et al. A three-dimensional (3DVAR) data assimilation system for use with MM5: Implementation and initial results [J]. Mon Wea Rev, 2004, 132: 897-914.

[6] LIAO Jie, TAN Zhe-min. Numerical simulation of a heavy rainfall event along the meiyu front: Influences of different scale weather systems [J]. Acta Meteorol Sinica, 2005, 63 (5): 771-789 (in Chinese).

[7] JOLLIFFE I T, STEPHENSON D B. Forecast Verification. A Practitioner's Guide in Atmospheric Science [M]. Chichester: John Wiley & Sons Ltd, 2003, 1-240.

[8] WILKS D S. Statistical Methods in the Atmospheric Sciences (2nd ed) [M]. Burlington: Academic Press, 2005, 1-648.

[9] HOFFMAN R N, LIU Z, LOUIS J-F, GRASSOTTI C. Distortion representation of forecast errors [J]. Mon Wea Rev, 1995, 123: 2 758-2 770.

[10] EBERT E E, MCBRIDE J L. Verification of precipitation in weather systems: Determination of systematic errors [J]. J Hydrol, 2000, 239: 179-202.

[11] CASATI B, ROSS G, STEPHENSON D B. A new intensity scale approach for the verification of spatial precipitation forecasts [J]. Meteorol Appl, 2004, 11: 141-154.

[12] DAVIS C A, BROWN B G, BULLOCK R G. Object-based verification of precipitation forecasts, Part I: Methodology and application to mesoscale rain areas [J]. Mon Wea Rev, 2006, 134: 1 772-1 784.

[13] ROBERTS N M, LEAN H W. Scale-selective verification of rainfall accumulations from high-resolution forecasts of convective events [J]. Mon Wea Rev, 2008, 136: 78-97.

[14] TUSTISON B, HARRIS D, FOUFOULA-GEORGIOU E, Scale issues in verification of precipitation forecasts [J]. J Geophys Res, 2001, 106, D11: 775-784.

[15] THEIS S E, HENSE A, DAMRATH U. Probabilistic precipitation forecasts from a deterministic model: A pragmatic approach [J]. Meteorol Appl, 2005, 12: 257-268.

[16] EBERT E E. Fuzzy verification of high resolution gridded forecasts: A review and proposed framework [J]. Meteorol Appl, 2008, 15: 51-64.

[17] ROBERTS N M. Assessing the spatial and temporal variation in the skill of precipitation forecasts from an NWP model [J]. Meteorol Appl, 2008, 15: 163-169.

[18] MITTERMAIER M, ROBERTS N M. Intercomparison of spatial forecast verification methods: Identifying skillful spatial scales using the fractions skill score [J]. Wea Forecast, 2010, 25: 343-354.

[19] ZHANG M, ZHANG F, HUANG X, ZHANG X. Intercomparison of an ensemble Kalman filter with three- and four-dimensional variational data assimilation methods in a limited-area model over the month of June 2003 [J]. Mon Wea Rev, 2011, 139: 566-572.

Citation: ZHANG Xu-bin, TAN Zhe-min. Influence of different-scale errors interactions on analysis and forecast of regional NWP model [J]. J Trop Meteorol, 2015, 21(4): 374-388.